Journal of Alloys and Compounds 521 (2012) 134–140

Contents lists available at SciVerse ScienceDirect

Journal of Alloys and Compounds

journal homepage: www.elsevier.com/locate/jallcom

Far-infrared spectroscopy of $Cd_{1-x}Mn_xS$ quantum dots

R. Kostić[a], M. Petrović Damjanović[a], N. Romčević[a,*], M. Romčević[a], D. Stojanović[a], M. Čomor[b]

[a] Institute of Physics, University of Belgrade, P.O. Box 68, 11080 Belgrade, Serbia
[b] Vinča Institute of Nuclear Sciences, University of Belgrade, P.O. Box 522, 11000 Belgrade, Serbia

ARTICLE INFO

Article history:
Received 27 December 2011
Accepted 15 January 2012
Available online 27 January 2012

Keywords:
Nanostructured materials
Phonons
Semiconductors
Light absorption and reflection

ABSTRACT

Far-infrared reflectivity spectra, in spectral region 50–600 cm^{-1} and temperature region 80–300 K, of CdS and $Cd_{1-x}Mn_xS$ nanocrystals embedded in hexametaphosphate, are presented. The analysis of the far-infrared experimental reflectivity spectrum was made by the fitting procedure. The Maxwell–Garnet effective medium theory is used for modeling an effective dielectric function as well as to separate respond from nanoparticles.

To analyze spectra in CdS ω_{TO}(≈238 cm^{-1}) to ω_{LO}(≈305 cm^{-1}) spectral region, quantized dipolar modes in a spherical isotropic material quantum dot (QD) are considered in the framework of a continuum model. As to the mechanical boundary conditions rigid sphere is concerned. Experimental far-infrared reflectivity spectra of our samples are in general agreement with the predictions of this model.

Experimentally registered and through fitting procedure located features for CdS nanoparticles in spectral region below CdS ω_{TO} at: ≈102 cm^{-1}, ≈135 cm^{-1}, ≈170 cm^{-1} and ≈210 cm^{-1} are associated to defect induced modes, especially to defects located near the surface of CdS QD. In region over CdS ω_{LO}, modes are identified as multiphonons. In $Cd_{1-x}Mn_xS$ QD spectra new reflectivity peaks are at: ≈85 cm^{-1}, ≈110 cm^{-1} and ≈180 cm^{-1} in spectral region below CdS ω_{TO}, ≈270 cm^{-1} inside CdS ω_{TO}–ω_{LO} spectral region and ≈356 cm^{-1} and ≈376 cm^{-1} in region over CdS ω_{LO}. First two registered modes are associated to both mass and force constant defects at the surface, and rest four modes are consequence of MnS phases present in the sample.

1. Introduction

Vibrational spectroscopy (far-infrared and Raman) is a useful, non-destructive procedure sensitive to local environment, ideal for *in site* probing during growth, and during device fabrication and operation. In low-dimensional semiconductors optical phonon modes behave substantially different from those of bulk. Optical phonons confined in semiconductor QDs affect the electronic properties responsible for Raman scattering. Most of the experimental studies of optical phonons in QDs have been performed by Raman spectroscopy [1–5]. Quantum-size effect on optical phonons can also be seen by far-infrared (FIR) spectroscopy [6–10].

Diluted magnetic semiconductors (DMS) are alloys with magnetic ions diluted in nonmagnetic $A^{II}B^{VI}$ semiconductors. Mn^{2+} ions can be incorporated into an $A^{II}B^{VI}$ semiconductor host in large proportions without substantially altering the crystallographic quality of the material. Mn^{2+} has a relatively large magnetic moment due to the $3d^54s^2$ electronic configuration. Mn^{2+} is electrically neutral in an $A^{II}B^{VI}$ host, thus avoiding the formation of any acceptor or donor impurities in the crystal. In the nanometer-size, many of the physical properties of DMS are expected to be influenced by quantum confinement of the electronic states and hence differ from those of the bulk crystals. Magnetic properties of Mn^{2+} incorporated in CdS and ZnS nanoparticles are widely investigated [11,12]. Optical properties were studied, and fluorescence due to isolated Mn^{2+} ions in tetrahedral coordination was observed and attributed to a quantum size effect [13–15].

$Cd_{1-x}Mn_xS$ is DMS which belongs to a group of materials known as mixed crystals. Phonon spectra of mixed crystals depend of the properties of end members. It is known that CdS, end member in $Cd_{1-x}Mn_xS$ dominating in the case of small x, crystallize in wurtzite (as in our case) or sphalerite lattice structure. Bulk $Cd_{1-x}Mn_xS$ exists in wurtzite structure for x up to ~0.45 [16]. Vibrational spectra of pure CdS and mixed crystals with CdS as one end-member are well known [17]. Bulk CdS samples are very reflective between ω_{TO} = 240 cm^{-1} and ω_{LO} = 304 cm^{-1}, and flat with low reflectivity out of this region. Second end member, MnS appears in three crystallographic modifications [18]. One of them is α-MnS that crystallizes in the cubic structure of NaCl type. The TO(LO) frequencies of this phase are 185(330) cm^{-1} [19]. The zincblende crystallographic modification of MnS (β-MnS) has phonon frequencies of TO(LO) modes at 286(343) cm^{-1}. These phonon frequencies

* Corresponding author. Tel.: +381 11 3713 026; fax: +381 11 3713 531.
E-mail address: romcevi@ipb.ac.rs (N. Romčević).

0925-8388/$ – see front matter © 2012 Published by Elsevier B.V.
doi:10.1016/j.jallcom.2012.01.079

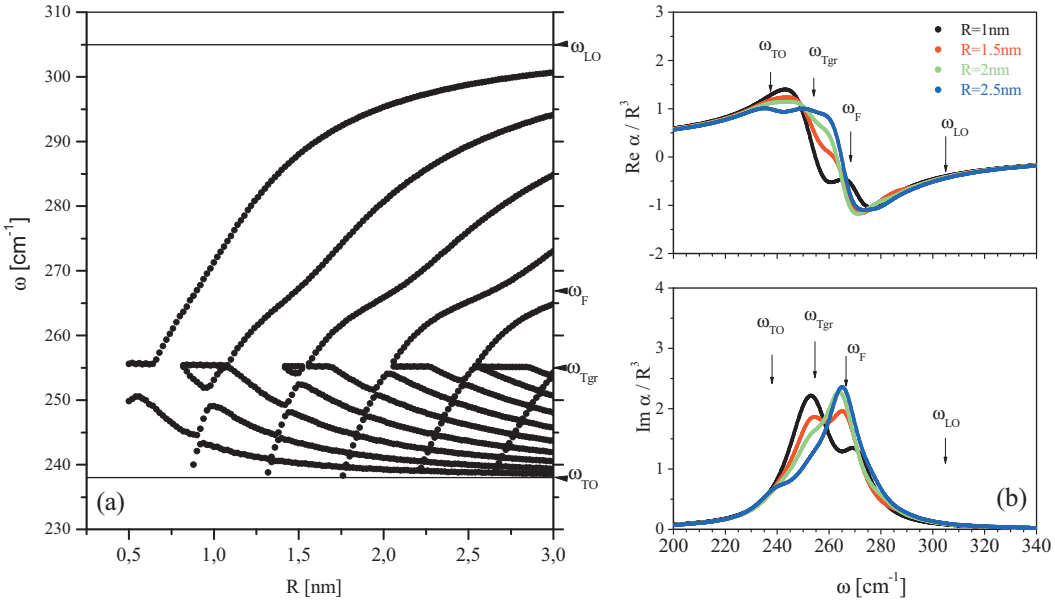

Fig. 1. (a) The radial dependence of $l = 1$ phonon frequencies calculated for CdS QDs (rigid boundary conditions) embedded in a matrix with $\varepsilon_2^\infty = 4$. The Fröhlich mode is at ≈267 cm^{-1}. (b) Real (up) and imaginary (down) parts of the polarizability for CdS spheres of different radii embedded in matrix with $\varepsilon_2^\infty = 4$.

were obtained from far-infrared reflectivity measurements of β-MnS thin films [20]. The phonon properties of zincblende MnS have been investigated in ZnS–MnS alloys [21]. Using the modified random element-isodisplacement (MREI) model, the TO(LO) mode frequencies of β-MnS were calculated at 293(361) cm^{-1}. Some investigations [22] show phonon frequency of zincblende MnS thick layers to be 380 cm^{-1}. The third modification of MnS is wurtzite MnS (γ-MnS), but this one is not of our interest here.

In studying vibrational modes of nanocrystals, knowledge of phonon dispersion of bulk material is required. For proper treatment of materials with dispersive phonons it is essential to satisfy mechanical as well as electromagnetic boundary conditions at the surface of particle. The group of authors [23] developed a theory for the optical vibrational modes of quantum dots (QDs) and showed that correct boundary conditions demand the coupling of longitudinal and transverse modes. The effect of correct mechanical boundary conditions is most significant to the smallest nanocrystals of materials with dissipative phonons.

In this paper we report results of experimental FIR reflectivity spectra of composites containing CdS and $Cd_{1-x}Mn_xS$ nanosize crystals. $Cd_{1-x}Mn_xS$ nanoparticles ($d \approx 4.5$ nm) of various compositions, $x = 0$, 0.01, 0.05, 0.1, 0.15, 0.3, were prepared by colloidal chemistry based procedure. We also presented results of theoretical studies of FIR active vibrations in spherical, nanosized CdS QDs. The phonon related polarizability of single CdS QD and effective dielectric function of composites containing QDs with narrow size distribution are calculated. The effects of QD dimension and volume fraction to effective dielectric function and consequently to reflectivity spectra, for this ideal case, are analyzed.

2. Synthesis and characterization of $Cd_{1-x}Mn_xS$ nanoparticles

Colloidal dispersions consisting of $Cd_{1-x}Mn_xS$ nanoparticles were prepared by mixing solution containing $Cd(NO_3)_2$ and $MnSO_4$ with solution containing Na_2S in the presence of surface active agent sodium hexametaphosphate $(NaPO_3)_6$. The concentration of cations ($[Cd^{2+}] + [Mn^{2+}]$) was constant and equal to 2×10^{-3} M, while an "excess" of S^{2-} ions was used in the synthesis (2.4×10^{-3} M). The content of Mn^{2+} ions was varied up to $x = 0.30$. The concentration of $(NaPO_3)_6$ was 2×10^{-2} M. The light and air were excluded during the preparation of colloidal dispersions. After precipitation of colloidal particles the solvent was removed by vacuum evaporation at room temperature. The obtained yellow powders could be redissolved in water to give a colloid with the same structured absorption spectrum as the solution before evaporation of the solvent. The contents of cations in powders consisting of $Cd_{1-x}Mn_xS$ nanoparticles were checked out by measuring atomic absorption (ICP-AS Perkin-Emer 6500). The X-ray diffraction analysis of $Cd_{1-x}Mn_xS$ nanoparticles performed for various compositions showed hexagonal wurtzite structure of CdS. UV–vis absorption spectra were recorded on Perkin-Elmer Lambda 5 instrument. A blue shift of the absorption onset of the CdS nanoparticles compared to bulk CdS was about 0.3 eV. The diameter of the particles was calculated using effective mass approximation model [24]. The calculated value for the diameter of CdS nanoparticles was found to be about 4.5 nm.

3. Quantized dipolar modes

A continuum model of the optical phonon confinement in a spherical QD treats properly both mechanical and electrostatic boundary conditions. This model, which uses parameters of bulk phonon dispersion curves, is limited to nanoparticles of regular shape made of bulk material. Although this is not the case in real nano-crystallites, we present results of calculation for ideal spherical CdS QD.

We assumed that particles are small spherical semiconductor crystals surrounded by matrix material. Materials are assumed to be isotropic and homogeneous, separated by the surface of the sphere. First, we considered one small spherical CdS crystal of radius R [25,26]. This consideration of confined optical vibrations in nanocrystals is based on macroscopic equation for the relative displacement ($\vec{u}$) of the positive and negative ions:

$$(\omega^2 - \omega_{TO}^2)\vec{u} = \beta_L^2 \vec{\nabla}(\vec{\nabla}\vec{u}) - \beta_T^2 \vec{\nabla} \times (\vec{\nabla} \times \vec{u}) + \frac{e_T \vec{\nabla}\varphi}{\rho v}. \quad (1)$$

The parameters of the equation are: ρ is the reduced mass density, ω_{TO} is the TO bulk frequency, $e_T = \sqrt{\varepsilon_1^\infty \mu v(\omega_{LO}^2 - \omega_{TO}^2)/(4\pi)}$ the transverse charge, v is the unit cell volume, and β_T and β_L

Table 1
Material parameters used in the calculation. CdS parameters are transferred from Refs. [27,28]. ε_2^∞ is assumed to be 4.

Parameters	CdS	Matrix
ω_{LO} (cm^{-1})	305	
ω_{TO} (cm^{-1})	238	
β_L ($m\,s^{-1}$)	3.6×10^3	
β_T ($m\,s^{-1}$)	1.58×10^3	
ε_1^∞	5.3	
ε_2^∞		4

are the phenomenological bending parameters for bulk dispersion curves. ε_1^∞ is the high frequency dielectric constant of the sphere. The second equation, which connects the electrostatic potential to the mechanical displacement, is:

$$\vec{\nabla}\left(\varepsilon_1^\infty\vec{\nabla}\varphi-\frac{4\pi e_T}{v}\vec{u}\right)=0. \tag{2}$$

These equations describe optical phonon dispersion curves of infinite isotropic material. Frequency-dependent bending parameters β_T^2 and β_L^2 are derivatives of corresponding dispersion curves, $|d\omega^2/dk^2|$, but in CdS case, according to the shape of dispersion curves [27,28] they are assumed as constant, Table 1. We assumed matrix is homogeneous material.

This problem is solved in spherical coordinates. The spherically symmetric solution of Eqs. (1) and (2) is:

$$\begin{aligned}
u^r &= \left[A_l\frac{dj_l(qr)}{dr}+B_l l(l+1)\frac{g_l(Qr)}{r}+C_l r^{l-1}\right]Y_{lm}(\theta,\phi),\\
u^\theta &= \left\{A_l j_l(qr)+B_l\frac{d[g_l(Qr)r]}{dr}+C_l r^l\right\}\frac{1}{r}\frac{\partial}{\partial\theta}Y_{lm}(\theta,\phi),\\
u^\phi &= \{\ldots\}\frac{1}{r\sin\theta}\frac{\partial}{\partial\phi}Y_{lm}(\theta,\phi),
\end{aligned} \tag{3}$$

where $q=\sqrt{(\omega_{LO}^2-\omega^2)/\beta_L^2}$, $Q=\sqrt{|(\omega_{TO}^2-\omega^2)|/\beta_T^2}$, j_l is the spherical Bessel function, Y_{lm} is the spherical harmonic and $g_l(z)=\begin{cases} j_l(z), \ldots, z^2\rangle 0\\ i^{-l}j_l(iz), \ldots, z^2\langle 0\end{cases}$. The constants A, B and C that determine the longitudinal, transverse and surface components of one confined vibration are determined by boundary conditions. Both, electrostatic (the continuity of the electrostatic potential and the normal component of the electric displacement) and mechanical (the continuity of all components of $\vec{u}$ and components of the stress tensor) conditions must be fulfilled at the surface. For mechanical boundary conditions usually two limiting cases are considered: a rigid sphere ($\vec{u}=0$ at the surface of the sphere) and free-standing sphere (all components of the stress tensor are zero at the surface). A rigid sphere approach is adequate if there is large separation between the optical branches of the two components. QDs of semiconductor embedded in glass, or in other semiconductor are such examples.

The equation for the frequencies of the spherical modes of a rigid sphere is:

$$\begin{aligned}
&qR\cdot j_l'(qR)\cdot\{\gamma\varepsilon_2^\infty[QR\cdot g_l'(QR)-l\cdot g_l(QR)]\\
&\quad+(l\varepsilon_1^\infty+(l+1)\varepsilon_2^\infty)[QR\cdot g_l'(QR)+g_l(QR)]\}\\
&\quad=l(l+1)\cdot j_l(qR)\cdot\{\gamma\varepsilon_2^\infty[QR\cdot g_l'(QR)-g_l(QR)]\\
&\quad+(l\varepsilon_1^\infty+(l+1)\varepsilon_2^\infty)g_l(QR)\},
\end{aligned} \tag{4}$$

where $\gamma=(\omega_{LO}^2-\omega_{TO}^2)/(\omega^2-\omega_{TO}^2)$ and R is QD radius.

The spherically symmetric solutions of Eq. (1) must belong to the irreducible representations of the three-dimensional rotation-inversion group $O(3)$ labeled as D_l^g (even) and D_l^u (odd upon inversion). The mixed modes belong to $D_0^g, D_1^u, D_2^g, \ldots$. The dipole operator responsible for FIR absorption belongs to D_1^u while Raman transition operator for dipole-allowed scattering belongs to D_0^g and D_2^g [29].

Frequencies of the spherical ($l=0$) and spheroidal quadrupolar modes ($l=2$) can be calculated, Eq. (4) and in principal observed by resonant Raman scattering [30–34].

In case $l=1$ solutions have both longitudinal and transversal components including a surface mode contribution. The dipolar mode frequencies, $l=1$, calculated as solutions of Eq. (4), for parameters from Table 1, are presented in Fig. 1(a). Solutions are placed between ω_{TO} and ω_{LO}.

Transversal and longitudinal dispersion curves of bulk CdS intersect inside Brillouin zone. The dispersion of the TO mode is positive and the TO confined modes have frequencies greater than the bulk ω_{TO} frequency. At the frequency of $\approx$255 cm^{-1}, ω_{Tgr}, the transverse wave vector component has a value of the edge of the Brillouin zone in bulk CdS. As the wave vector component for TO modes cannot be larger than this value it must be continued along the complex Brillouin zone. This complex wave vector effectively damps out the contribution of the TO modes to the dispersion relation. Above this frequency only contribution is due the confined LO modes with some bending in dispersion at $\approx$267 cm^{-1} caused by the interaction with the electrostatic surface mode contribution. Electrostatic surface mode for $l=1$ is known as Fröhlich mode (ω_F). This mode is not a solution of the rigid boundary conditions problem, but there is a bending in the dispersion curves near to ω_F, as can be seen in Fig. 1.

Composite of QDs and matrix is an example of inhomogeneous medium and an effective response of this composite is measured in the FIR spectral region. To calculate effective dielectric response we must determine polarizability of a single spherical inclusion, i.e. one QD.

Polarizability α of a single QD is a sum of a "background" polarizability (α_0) and frequency dependent part (α_1) which is a consequence of the forced dipolar vibrations induced in the sphere by the field [33]:

$$\alpha=\alpha_0+\alpha_1=\frac{\varepsilon_1^\infty-\varepsilon_2^\infty}{\varepsilon_1^\infty+2\varepsilon_2^\infty}R^3+\frac{3\varepsilon_1^\infty\varepsilon_2^\infty(\omega_{LO}^2-\omega_{TO}^2)}{(\varepsilon_1^\infty+2\varepsilon_2^\infty)^2}\sum_n\frac{D_n^2}{\omega_n^2-\omega^2-i\delta}. \tag{5}$$

ω_n are solutions of Eq. (4) for $l=1$ presented in Fig. 1(a). δ reflects the value of damping factor. $D_n=\int_0^R(u_n^r+2u_n^\theta)r^2dr$, where u_n^r and u_n^θ are radial dependent parts of the displacement components u^r and u^θ, Eq. (3), for nth solution. D_n is measure of the contribution of nth mode to polarizability, i.e. the strength of each mode. Coefficients D_n must fulfill condition: $\sum_n|D_n|^2=R^3$.

Calculated values of D_n give us opportunity to form a frequency dependent polarizability of sphere. Results of our calculation for real and imaginary part of polarizability are presented in Fig. 1(b). For the smallest radius, $R=1$ nm, group of modes close to the bulk TO frequency produce the dominant one of two polarizability peaks. In principal there is multimodal structure of polarizability of sufficiently small sphere. As R increases number of confined modes increases to, and modes close to the Fröhlich frequency ($\omega_F\approx267\,cm^{-1}$) produce the most of the polarizability, i.e. of the FIR activity. For $R=2.5$ nm multimodal structure is almost absent and one structure close to ω_F dominates.

In case of spherical QDs, volume filling fraction f cannot be greater than ~0.5. Filling fraction of the many experimentally studied QD composites does not exceed few percent. To illustrate behavior of the ideal system we present results for three different filling fractions: 0.05 and 0.2 for spheres of one dimension (without size distribution) uniformly distributed inside sample. For small filing fraction f, inclusions of QD material are completely surrounded by a uniform matrix, the effective medium approach originally due to Maxwell–Garnett can be used to describe effective dielectric function [33]. The real and imaginary parts of effective dielectric function, calculated for composites containing assumed

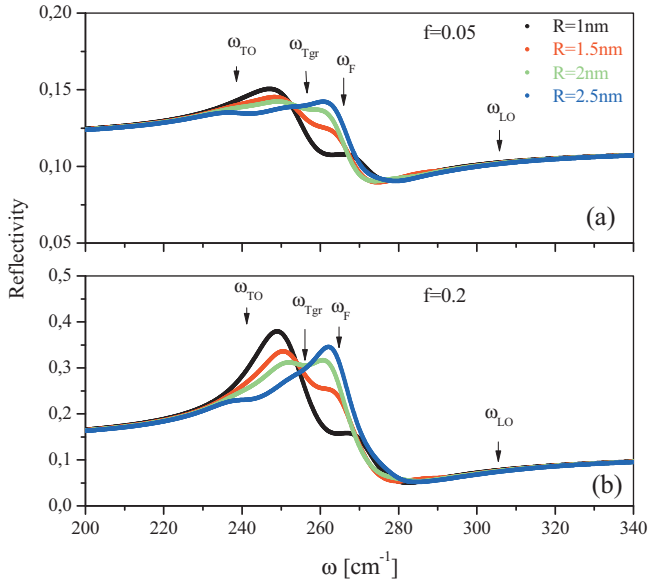

Fig. 2. Calculated reflectivity of composite containing (a) $f = 0.05$ and (b) $f = 0.2$ of CdS QDs of different radii.

volume fraction of CdS QDs of different sizes, give reflectivity spectra in Fig. 2. Increase of filling fraction f increases the intensity of reflectivity.

We conclude that in the case of $R < 2.5$ nm there will be two maximums or one maximum and a shoulder in reflectivity spectra. Modes of frequency $\omega < \omega_{gr}$ produce spectral structure in reflectivity in region 240–260 cm^{-1}, that dominate in $R = 1$ nm QD spectra, and modes in spectral region $\omega > \omega_{gr}$ produce structure in region 260–280 cm^{-1}, that dominate in $R = 2.5$ nm QD spectra, Fig. 2. In case $R \gg 2.5$ nm there will be one maximum in reflectivity approximately at the position ≈ 265 cm^{-1}.

For large filling fraction dipole–dipole interaction between QDs can be important. It can modify the FIR spectrum and absorption band can be shifted from Fröhlich frequency toward the bulk TO frequency [33]. In this approach maximum in reflectivity is pushed toward ω_{TO} or even below ω_{TO}. Such behavior of the spectrum imply large filling factor at least in a part of sample. Theory applied in this work, allowed a good description of experimental results in Refs. [30–33], or absorption spectrum of PbS QDs embedded in PPV [35]. No quantum size effect is expected for free-standing QD, where the size-independent Fröhlich mode is allowed.

4. Results and discussion

Experimental reflectivity spectra of $Cd_{1-x}Mn_xS$ nanoparticles ($x = 0$, 0.01, 0.05, 0.1, 0.15, 0.3) embedded in $(NaPO_3)_6$, and spectrum of matrix, i.e. pure $(NaPO_3)_6$ in the wave number range from 50 to 600 cm^{-1} at 300 K and 80 K are given by the points in Fig. 3. As a consequence of small density of CdS nanoparticles in our samples the change of reflectivity compared to spectra of matrix alone is not drastic. It is difficult to identify peaks without detailed analysis. All spectral features are more prominent in case $T = 80$ K, especially in case of higher Mn content.

The analysis of the experimental far-infrared reflectivity spectra was made by the fitting procedure. The Maxwell–Garnet effective medium theory is used for modeling an effective dielectric function. This classical mixture formula is applied to homogeneous, spherical or ellipsoidal inclusions in a homogeneous, isotropic or anisotropic background material [36]. The mixture we studied consists of two component: one is treated as host, in our case $(NaPO_3)_6$, of dielectric function ε_b and the other as an inclusion phase ($Cd_{1-x}Mn_xS$) with dielectric function ε_i. Both dielectric functions are described by:

$$\varepsilon_{i,b}(\omega) = \varepsilon_\infty \left(\prod_{k=1}^{n} \frac{\omega^2 + i\gamma_{LOk}\omega - \omega_{LOk}^2}{\omega^2 + i\gamma_{TOk}\omega - \omega_{TOk}^2} - \frac{\omega_P^2}{\omega(\omega + i\tau^{-1})} \right) \quad (6)$$

where ω_{TO}, ω_{LO} and ω_P are transverse, longitudinal and plasma frequencies, respectively. γ_{TO} and γ_{LO} are the damping of TO and LO modes, τ is the free-carrier relaxation time and ε_∞ is the high frequency dielectric constant. The first term in (6) comes from the lattice vibration contribution to the dielectric constant. The second term comes from the free carrier contribution to the dielectric constant. The volume fraction of the inclusions is $f = 4\pi n R^3/3$, where n is the particle number density and R is sphere radius.

The Maxwell–Garnett formula is explicitly given by:

$$\varepsilon_{eff} = \varepsilon_b + \frac{3f\varepsilon_b(\varepsilon_i - \varepsilon_b)}{\varepsilon_i + 2\varepsilon_b - f(\varepsilon_i - \varepsilon_b)} \quad (7)$$

where ε_{eff} is the effective dielectric function of the mixture, and gives the best results for the small volume fraction (see for example Ref. [36]). Through fitting procedure we get parameters of series of modes. Calculated reflectivity curves for these parameters are shown by lines in Fig. 3. Position of modes as function of x for temperatures 300 K and 80 K is given in Fig. 4. Modes are separated into two groups. In Fig. 4(a) there are modes that are present in all samples. Presence of these modes in case $x = 0$, i.e. in CdS QDs imply that they are characteristic for CdS QD and we analyzed them in that manner. In $Cd_{1-x}Mn_xS$ QD spectra there are additional modes that are separately presented in Fig. 4(b).

In previous chapter we predicted behavior of the system in ideal case, but in reflectivity spectra of our samples there are lot of modes out of the CdS optical phonon region. If shape of interfaces is so irregular spherical assumption can be ruined, or some parts of interface, as peninsulas can be new space of confinement. Another discrepancy from ideal case is also matrix inhomogeneity, i.e. fluctuating properties of the matrix in real samples. Assumed parameters for QD material were the same in all directions of Brillouin zone. These parameters are good approximation for wurtzite crystal structure for the Γ–A direction in the Brillouin zone which is not far from the cubic in this case. Four atoms per wurtzite primitive cell have more degree of freedom and corresponding phonon dispersions, with characteristic high density of states at the end of Brillouin zone ($M_1 \approx 130$ cm^{-1}, $M_4 \approx 170$ cm^{-1}, H_3,$M_1 \approx 210$ cm^{-1}). We, also, assumed perfectly crystalline spherical particles. Disorder is hard to avoid in nano-structured materials.

In our analysis we separated spectral region into three regions: $\omega < \omega_{TO}$ CdS, $\omega_{TO} < \omega < \omega_{LO}$ and $\omega > \omega_{LO}$.

In the second region, in the spectra of CdS QDs there are two modes. According to the fitting procedure TO/LO frequencies of these two modes are: ≈230/256 cm^{-1} and ≈285/295 cm^{-1}, Figs. 3 and 4(a). This is in agreement to results of calculations given in Section 3. Absence of the multimodal structure is predicted, i.e. dimension of the CdS QDs ($R \approx 2.25$ nm) is not small enough to produce multimodal behavior in reflectivity spectra. As predicted, in optical phonon confinement region of $R < 2.5$ nm CdS QD radius we expect two structures in reflectivity spectra: one in the region $\omega < \omega_{Tgr}$ and the other in the region $\omega > \omega_{Tgr}$. For $R < 2$ nm the first one is expected to be of higher reflectivity giving slope similar to the experimental. For $R > 2$ nm the second one is expected to be of higher reflectivity giving slope opposite to the experimental one. There are few possible reasons that can be responsible for obtained experimental slope of reflectivity. One is the presence of QDs of smaller radius. Second is existence of regions in sample with higher concentrations of QDs implying dipole–dipole interaction. It is hard to control spatial positions of QDs in order to have uniform QD distribution, and in our samples uniformity of QD distribution in

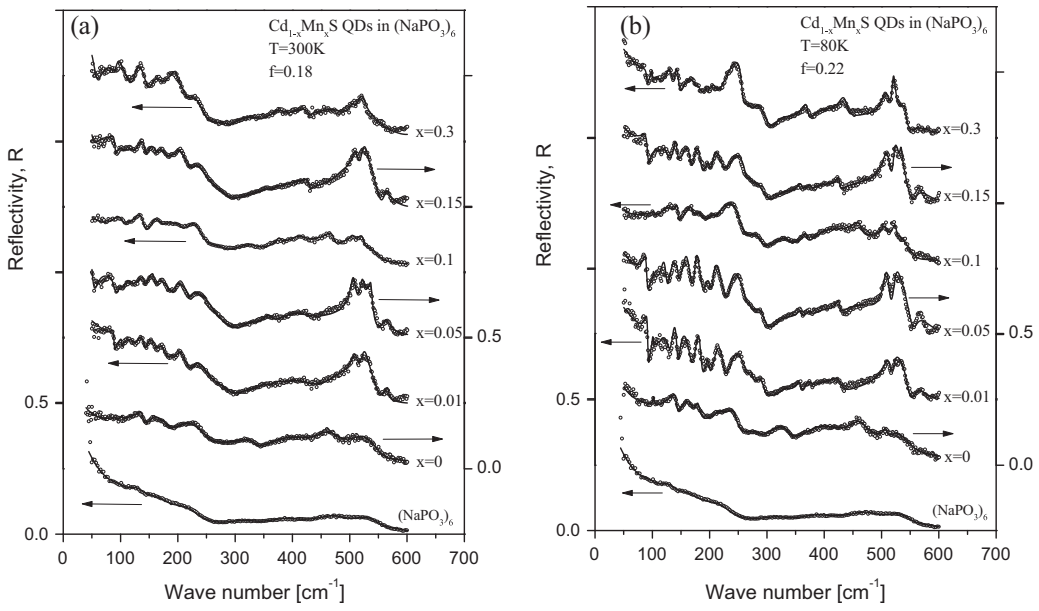

Fig. 3. FIR reflectivity spectra of CdS and $Cd_{1-x}Mn_xS$ QDs at $T = 300$ K (a) and $T = 80$ K (b). The experimental spectra are represented by circles. The solid lines are calculated spectra obtained using fitting procedure based on the model given by Eqs. (6) and (7).

matrix is questionable. Finally, existence of additional mode of frequency 220 cm^{-1}, practically at the edge of this region is probably the most important one.

In the first region, where IR reflectivity spectra of bulk CdS, or ideal shaped CdS QD embedded in homogeneous matrix of constant dielectric permittivity should be almost flat, in experimental spectra of CdS QDs there are four spectral structures at: ≈102 cm^{-1}, ≈135 cm^{-1}, ≈170 cm^{-1} and ≈210 cm^{-1}, Figs. 3 and 4(a).

The first mode at about 102 cm^{-1} is the result of Cd vacancies [37].

Group of authors [38] proposed a model to investigate the impact of QD shape irregularities and the interatomic force constant's disorder in a semiconductor nano-crystallites. They studied dynamical problem in two-dimensions. The nearest-neighbor interaction constant could be considered as random variable within a certain distribution in order to model random atomic deviations from the regular lattice positions. Applying free b.c.s. produce a mode below ∼210 cm^{-1}.

Phonon properties of diatomic crystals in some symmetry directions can be properly described even by one-dimensional, linear diatomic chain [42], and even better by dynamical problem in two dimensions (2D) [38]. The obtained results are in good quantitative agreement with the more complex three-dimensional calculations. For wurtzite structure, with four atoms per primitive cell, Γ–A direction allows such modeling with additional zone folding. In studying vibrational modes of nanocrystals, knowledge of phonon dispersion of bulk material is required. In the spectral region where IR reflectivity spectrum of bulk material is flat, new structures are a consequence of disorder emphasized by finite, i.e. nanometer, size of the crystals. In the nanometer size CdS QDs, that are subject of this investigation, about 50% of atoms are on the surface, which induces more probable defect creation. We modeled these nanocrystals with finite two-dimensional problem [38]. Force constants in the assumed system of internal vibration coordinates from bulk are transferred to finite 2D problem. We tentatively assumed circular 2D area. We modeled edge of area to be occupied by one

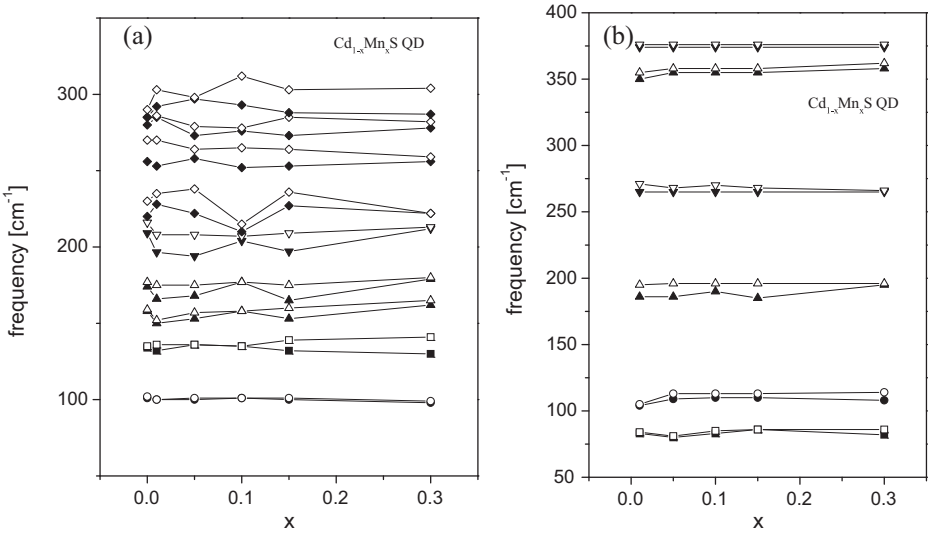

Fig. 4. Phonon frequencies of CdS and $Cd_{1-x}Mn_xS$ QDs ($T = 300$ K (solid symbols) and $T = 80$ K (open symbols)) calculated by model described by Eqs. (6) and (7), obtained as a best fit: (a) phonons originated from CdS QDs and (b) additional phonons in spectra of $Cd_{1-x}Mn_xS$ QDs.

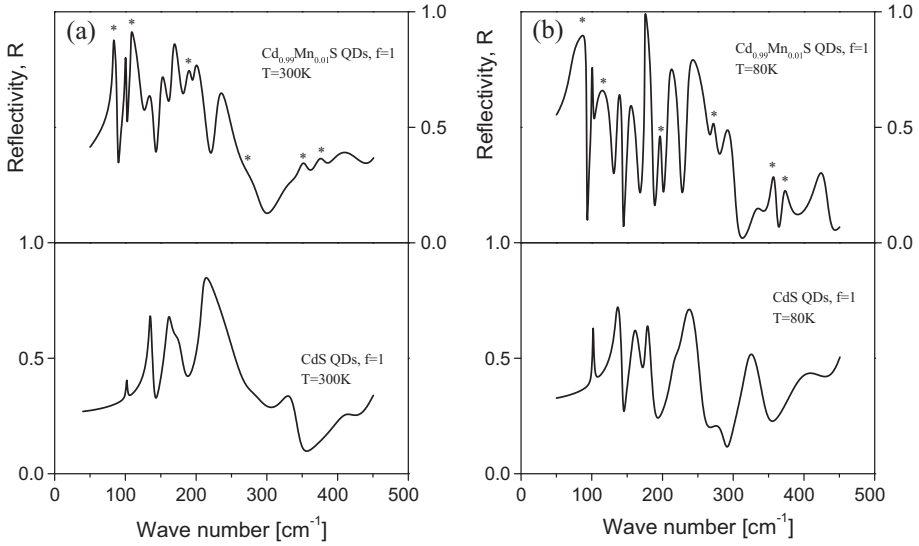

Fig. 5. Reflectivity spectra of $Cd_{1-x}Mn_xS$ QDs, obtained with $f = 1$ in Eq. (7), using the parameters obtained for the best fit.

sort of atoms and choose motion conditions and neighbors force constants between ending and neighbor atoms to identify frequencies registered in experimental spectra.

If we treat finite 2D area with ending Cd atoms and no motion at the end, that corresponds to rigid boundary conditions on the surface, with reasonable change in force constants for bonds toward ending atoms, we obtained frequencies from phonon branches of CdS out of the center and close to the end of Brillouin zone, at $\sim 170\,cm^{-1}$. If S atoms are placed at the end of the array, with no restriction in motion, assuming force constant between ending S atom and neighbor Cd atom to decrease in comparison to force constants inside array, the frequency of $\sim 135\,cm^{-1}$ is obtained.

In clusters with strongly disordered shape the appearance of low-frequency mode originating from Brillouin zone edge acoustic vibrations so called disorder activated acoustic modes is already seen [39–41]. Mode at $\sim 135\,cm^{-1}$ is practically disorder activated acoustic mode. We emphasize that this disorder is connected to the surface.

In the region above ω_{LO}, there are spectral features that can easy be identified as multiphonon features. We will discuss these modes at the end of this chapter.

In tentatively doped semiconductor phase there are new sources of disorder. Despite the initial doping conditions nanoparticles in the sample slightly differ in properties as consequence of fluctuation in composition. In $Cd_{1-x}Mn_xS$ QD reflectivity spectra new reflectivity peaks are at: $\approx 85\,cm^{-1}$, $\approx 110\,cm^{-1}$, $\approx 180\,cm^{-1}$, $\approx 270\,cm^{-1}$, $\approx 356\,cm^{-1}$, and $\approx 376\,cm^{-1}$.

In ideal case Mn^{2+} ions are well dispersed inside $Cd_{1-x}Mn_xS$ nanocrystals. For small x Mn ions should be isolated in tetrahedral coordination. It is shown [12] that there is a trend for Mn^{2+} ions to migrate to the nanocrystal surface.

Phonons of $Cd_{1-x}Mn_xS$ nanocrystals were modeled as a finite 2D area, also. We tentatively locate Mn^{2+} ions near the edge of area and choose force constants to get the characteristic frequencies. If Cd atoms are substituted by Mn atoms in different positions inside the area, the calculated frequencies belong to the region of the vibrational modes of CdS. That is a consequence of relation between atom masses and force constants corresponding to bulk materials. If Mn atoms are placed at the edge, which simulates Mn atom placed on the surface of the nanocrystal, calculated frequencies are in a region already abundant in modes. If S atoms are placed at the edge of array and Mn^{2+} ions as the first neighbors and force constants changing within reasonable limits, $\approx 85\,cm^{-1}$ and $\approx 115\,cm^{-1}$ frequencies are obtained. With increased amount of Mn, these characteristic frequencies are increased insignificantly. On the basis of this analysis we assigned these modes to modes connected to Mn^{2+} ions located near the surface.

Two pairs of TO(LO) frequencies, $186(356)\,cm^{-1}$ and $270(376)\,cm^{-1}$, correspond to α-MnS and β-MnS, respectively. We suppose that small areas of MnS are present in sample. Differences compared to the TO(LO) frequencies in bulk MnS are consequence of small dimension or phonon–plasmon interaction.

To emphasize position of the modes in spectra in Fig. 3 we artificially put filling factor f to be 1. We present hypothetical reflectivity spectra of two QD compositions in Fig. 5 just as an illustration.

In the region above $300\,cm^{-1}$, there are spectral features that can be easy identified as multiphonon features. Multiphonon processes in CdS based materials were registered [41] and discussed in detail [42]. Raman spectra were analyzed in detail but these processes can also be registered in FIR measurements [32], as in our work. A decrease in particle dimensions increases these effects. In our spectra dominant structure is in the region from 470 to $540\,cm^{-1}$. In this region the frequencies are situated at: $4 \times 130 = 520\,cm^{-1}$, $3 \times 170 = 510\,cm^{-1}$, $4 \times 120 = 480\,cm^{-1}$, and $2 \times 240 = 480\,cm^{-1}$. These structures are intensive compared to the rest of spectra. Also, less intensive structures at $240 + 300 = 540\,cm^{-1}$, $2 \times 170 = 340\,cm^{-1}$, $300 + 130 = 430\,cm^{-1}$ and $240 + 170 = 410\,cm^{-1}$ are present in the spectra. Various models have been used to explain the multiphonon processes including the cascade model [43] and solid state analog of the configuration coordinate model [44]. Which of these spectral structures are intensive enough to be registered in experimental spectra depends on many factors, such as density of particles on surface of prepared tablet, for example. For these reasons it is very difficult to discuss the intensities of these multiphonon structures.

5. Conclusion

In this paper we present experimental far-infrared reflectivity spectra of CdS and $Cd_{1-x}Mn_xS$ QDs embedded in matrix of low reflectivity. As a result of the Maxwell–Garnet effective medium theory, followed by very careful fitting procedure, series of modes are identified in experimental spectra.

Calculations of quantized dipolar modes in ideal spherical CdS QD in the framework of a continuum model with rigid boundary conditions were performed. Two spectral structures are predicted

in reflectivity spectra of ≈4.5 nm diameter CdS QD in optical phonon region. Experimental reflectivity spectra, not so prominent in this spectral region, are generally in agreement with results of these calculations. This is hard to see without detailed analysis of experimental spectra. Spectral structures of different origin that dominate in the spectra are mostly out of this spectral region but some are at the edge of the optical phonon region.

For CdS QD there are four modes in spectral region below ω_{TO}, at: ≈102 cm^{-1}, ≈135 cm^{-1}, ≈170 cm^{-1} and ≈210 cm^{-1}. Positions of registered modes can be obtained as solutions of finite dynamical problem with different dynamical parameters at the surface compared to the parameters inside area. We tentatively assigned these modes as surface, i.e. surface disorder activated modes.

In $Cd_{1-x}Mn_xS$ QD spectra new reflectivity peaks are at: ≈85 cm^{-1}, ≈110 cm^{-1} and ≈180 cm^{-1} in spectral region below CdS ω_{TO}, ≈270 cm^{-1} inside CdS ω_{TO}–ω_{LO} spectral region and ≈356 cm^{-1} and ≈ 376 cm^{-1} in region over CdS ω_{LO}. First two modes registered in spectral region below CdS ω_{TO} can be connected to Mn^{2+} ions located near the surface, because they are solutions of dynamic problem for the finite dimension with both mass, Mn substitutes Cd, and force constant defects at the surface. Rest four modes are consequence of MnS phases present in the samples.

Spectral structures in the region above CdS ω_{LO} are identified as multiphonon features.

Acknowledgment

This work is supported by the Serbian Ministry of Education and Science under Project No. III45003 and III45020.

References

[1] M. Cardona, in: M. Cardona, G. Guntherodt (Eds.), Light Scattering in Solids II, Topics in Applied Physics, vol. 50, Springer-Verlag, Berlin, 1982.
[2] A.L. Rogach, Semiconductor Nanocrystal Quantum Dots, Springer-Verlag, Wien, 2008.
[3] A.A. Arora, M. Rajalakshmi, T.R. Ravindran, V. Sivasubramanian, J. Raman Spectrosc. 38 (2007) 604.
[4] M.I. Vasilevskiy, C. Trallero-Giner, Phys. Status Solidi B 247 (6) (2010) 1488.
[5] A. Rolo, M.I. Vasilevskiy, J. Raman Spectrosc. 38 (2007) 618.
[6] M.I. Vasilevskiy, A.G. Rolo, M.V. Artemyev, S.A. Filonovich, M.J.M. Gomes, Yu.P. Rakovich, Phys. Status Solidi B 224 (2001) 299.
[7] A.I. Belogorokhov, I.A. Belogorokhov, R.P. Miranda, M.I. Vasilevskii, S.A. Gavrilov, J. Exp. Theor. Phys. 104 (1) (2007) 111.
[8] V. Sivasubramanian, A.K. Arora, M. Premila, C.S. Sundar, V.S. Sastry, Physica E 31 (2006) 93.
[9] R. Kostić, M. Romčević, N. Romčević, L. Klopotowski, J. Kossut, J. Kuljanin, M.I. Čomor, J. Nedeljković, Opt. Mater. 30 (2008) 1177.
[10] N. Romčević, M. Romčević, R. Kostić, D. Stojanović, A. Milutinović, G. Karczewski, R. Galazka, J. Alloys Compd. 481 (2009) 6.
[11] B. Babić Stojić, D. Milivojević, M. Čomor, V. Vodnik, J. Phys.: Condens. Matter 16 (2004) 4625.
[12] L. Levi, N. Feltin, D. Ingert, M.P. Pileni, J. Phys. Chem. B 101 (1997) 9153–9160.
[13] A. Nag, D.D. Sarma, J. Phys. Chem. C 111 (37) (2007) 13624.
[14] B. Tripathi, F. Singh, D.K. Avasthi, D. Das, Y.K. Vijay, Physica B 400 (2007) 70.
[15] M. Romčević, N. Romčević, R. Kostić, L. Klopotowski, W. Dobrowolski, J. Kossut, M.I. Čomor, J. Alloys Compd. 497 (2010) 46.
[16] Y. Wang, N. Herron, T. Bain, Solid State Commun. 77 (1991) 33.
[17] M.A. Nusimovici, M. Balkanski, Phys. Rev. B 1 (2) (1970) 603.
[18] A. Pajaczkowska, Prog. Cryst. Growth Charact. 1 (1978) 289.
[19] D.R. Huffman, R.L. Wild, Phys. Rev. 156 (1967) 989.
[20] E. Jahne, O. Goedge, V. Weinhold, Phys. Status Solidi B 146 (1988) K157.
[21] A. Anastassiadou, E. Liarokapis, E. Anastassakis, Solid State Commun. 69 (1989) 137.
[22] L. David, X. Tang, G. Beamson, D. Wolverson, K.A. Prior, B.C. Cavenett, Phys. Status Solidi B 241 (3) (2004) 471.
[23] T.D. Krauss, W. Wise, Phys. Rev. Lett. 76 (8) (1996) 1336.
[24] L.E. Brus, J. Chem. Phys. 80 (1984) 4403.
[25] R. Roca, C. Trallero-Giner, M. Cardona, Phys. Rev. B 49 (1994) 13704.
[26] M.P. Chamberlain, C. Trallero-Giner, M. Cardona, Phys. Rev. B 51 (1995) 1680.
[27] M.A. Nusumovichi, J.L. Birman, Phys. Rev. 156 (3) (1967) 925.
[28] H.W. Verleur, A.S. Barker, Phys. Rev. 155 (3) (1967) 750.
[29] E. Duval, Phys. Rev. B 46 (1992) 5795.
[30] M.I. Vasilevskiy, A.G. Rolo, M.J.M. Gomes, Solid State Commun. 104 (1997) 381.
[31] M.I. Vasilevskiy, A.G. Rolo, M.J.M. Gomes, Microelectron. Eng. 43–44 (1988) 715.
[32] A.G. Rolo, M.I. Vasilevsky, M.J.M. Gomes, O.V. Vikhrova, Yu.P. Rakovich, M.V. Artemyev, Mater. Res. Soc. Symp. Proc. 571 (2000) 217.
[33] M.I. Vasilevskiy, Phys. Rev. B 66 (2002) 195326.
[34] N. Romčević, R. Kostić, M. Romčević, M.I. Čomor, J.M. Nedeljković, J. Phys. D: Appl. Phys. 38 (2005) 1.
[35] T.D. Krauss, F.W. Wise, D.B. Tanner, Phys. Rev. Lett. 76 (8) (1996) 1376.
[36] A. Sihvola, Electromagnetic Mixing Formulae and Applications, IEE Electromagnetic Waves Series, vol. 47, Institution of Electrical Engineers, 1999, p. 1.
[37] J. Cebulski, E.M. Sheregii, J. Polit, A. Marcelli, M. Piccinini, A. Kisiel, I.V. Kucherenko, R. Triboulet, Appl. Phys. Lett. 92 (2008) 121904.
[38] M.I. Vasilevskiy, A.G. Rolo, M.J.M. Gomes, O.V. Vikharova, C. Ricolleau, J. Phys.: Condens. Matter 13 (2001) 3491.
[39] A.A. Sirenko, M.K. Zundel, T. Ruf, K. Eberl, M. Cardona, Phys. Rev. B 58 (1998) 12633.
[40] A. Ingale, K.C. Rustagi, Phys. Rev. B 58 (1998) 7197.
[41] R.C.C. Leite, J.F. Scott, T.C. Damen, Phys. Rev. Lett. 22 (1969) 780.
[42] Raman Scattering in Materials Science, in: W.H. Weber, R. Merlin (Eds.), in: Springer Series in Material Science, 2000.
[43] R.M. Martin, C.M. Varma, Phys. Rev. Lett. 26 (1971) 1241.
[44] R. Merlin, G. Guntherodt, R. Humphreys, M. Cardona, R. Suryanayanan, F. Holtzberg, Phys. Rev. B 17 (1978) 4951.